Journal of Food Bioactives
International Society for Nutraceuticals and Functional Foods
Original Research
J. Food Bioact. 2024;25:81–94

In silico ADME and molecular simulation studies of pharmacological activities of phytoconstituents of *Annona muricata* (L.) Fruit

Iseoluwa Isaac Ajayi[a], Toluwase Hezekiah Fatoki[b*], Ayodele Sunday Alonge[a], Courage Dele Famusiwa[c], Ibrahim Olabayode Saliu[d], Olapade Samuel Akinlolu[e], Chinemelum Adaora Onodugo[c] and Rachel Temitope Ojo[a]

[a]Department of Biological Sciences, Bamidele Olumilua University of Education, Science and Technology Ikere-Ekiti, Ekiti State, Nigeria
[b]Applied Bioinformatics Laboratory, Department of Biochemistry, Federal University Oye-Ekiti, Ekiti State, Nigeria
[c]Phytomedicine and Molecular Toxicology Research Laboratory, Department of Biochemistry, Federal University Oye-Ekiti, Ekiti State, Nigeria
[d]Department of Neuroscience, Washington University School of Medicine, St. Louis, MO, United States
[e]Department of Chemistry, Federal University Oye-Ekiti, Ekiti State, Nigeria
[*]**Corresponding author:** Toluwase Hezekiah Fatoki, Applied Bioinformatics Laboratory, Department of Biochemistry, Federal University Oye-Ekiti, Ekiti State, Nigeria. E-mail: toluwase.fatoki@fuoye.edu.ng
DOI: 10.31665/JFB.2024.18374
Received: February 03, 2024; **Revised received & accepted:** February 27, 2024
Citation: Ajayi, I.I., Fatoki, T.H., Alonge, A.S., Famusiwa, C.D., Saliu, I.O., Akinlolu, O.S., Onodugo, C.A., and Ojo, R.T. (2024). *In Silico* ADME and molecular simulation studies of pharmacological activities of phytoconstituents of *Annona muricata* (L.) Fruit. J. Food Bioact. 25: 81–94.

Abstract

Annona muricata Lin is known for its ethnomedicinal uses as food, decoctions, or infusions to address various conditions like skin infections, fever, diabetes, insomnia, malaria, hypertension, nervous disorders, diarrhea, and cancer. The study aimed to analyze the phytochemicals such as acetogenins, alkaloids, cyclopeptides, and flavonoids, present in *A. muricata* fruit, evaluate their pharmacokinetics, and understand binding dynamics with key molecular targets relevant to human well-being. Results indicated a mix of high and low gastrointestinal absorption (GIA) among *A. muricata* phytochemicals, with some demonstrating blood-brain barrier (BBB) permeability. Molecular target prediction highlighted frequent interactions with Programmed cell death protein 4 (PDCD4). Protein-protein interaction analysis revealed central connectivity of tyrosinase (TYR), Tyrosine 3-monooxygenase (TH), interleukin 2 (IL2), and others. Molecular docking results identified Luteolin 3,7-di-O-glucoside with the highest binding affinity for PDCD4 (−7.65 kcal.mol^{-1}), followed by Annonaine (−7.294 kcal.mol^{-1}); meanwhile, Dexamethasone (standard compound) exhibited a binding affinity of −6.682 kcal.mol^{-1}. Molecular dynamic simulation indicated a stable binding energy ΔGbind (Total) for the Annonaine - PDCD4 complex (−35.851 kcal.mol^{-1}) and Dexamethasone - PDCD4 complex (−28.489 kcal.mol^{-1}). In conclusion, this study suggests potential anticancer properties of *A. muricata* based on modulation of PDCD4 protein, influencing the CDK/Akt/STAT3 pathway. Further *in vivo* investigations are necessary to validate these findings.

Keywords: *A. muricata*; Phytoconstituents; Muricatocin A; Muricatetrocin B; PDCD4; anticancer.

1. Introduction

Annona muricata Lin., commonly referred to as soursop, is a member of the Annonaceae plant family and is extensively cultivated in tropical and subtropical regions, including Southeast Asia, South America, and the rainforests of Africa (Mutakin et al., 2022). The various plant parts of *A. muricata* L, encompassing leaves, bark, fruit, and seeds, have been traditionally used for ethnomedicinal purposes to address a diverse range of health issues (Mutakin et al., 2022; Nwonuma et al., 2023).

A. muricata is known for containing compounds with pharmacological activity, such as flavonoids, terpenoids, saponins, coumarins, lactones, anthraquinones, glycosides, tannins, and phytosterols, as identified in its leaf extract (Gavamukulya et al., 2014). The plant harbors approximately 100 phytochemicals distributed across its various parts (Mutakin et al., 2022). Notably, all parts of *A. muricata*, including fruit, stem, leaf, seed, root, and twigs, exhibit specific anticancer properties. These properties are believed to involve the inhibition of matrix metallopeptidases (MMP-2 and MMP-9), induction of apoptosis by enhancing caspase-3 expression, and modulation of the Bax/Bcl-2 ratio with cell cycle arrest at G0/G1 phase (Pieme et al., 2014; Moghadamtousi et al., 2014; Yang et al., 2015; Abdullah et al., 2017; Indrawati et al., 2017; Kim et al., 2018; Drishya et al., 2020; Hadisaputri et al., 2021).

This study adopts a comprehensive computational approach to unveil the inherent pharmacological importance of *A. muricata*, offering insights that are challenging to obtain in wet labs. Computational methods play a crucial role in expanding the understanding of the plant's medicinal applications and its mechanism of action. Previous computational studies have explored *A. muricata's* potential in treating hypertension by targeting angiotensin I converting enzyme (Suhandi et al., 2022), and antimalarial effect by analyzing interaction with six *Plasmodium falciparum* proteins (Nwonuma et al., 2023). Computational study of anti-prostate cancer potential of showed binding affinities between - 9.854 and 8.179 kcal.mol^{-1} for Human steroid 5′-reductase 2 enzyme, and that the binding free energy was in a range of −83.14 to −100.06 kcal.mol^{-1} (Apeh et al., 2023). Molecular docking results of the study of hypoglycemic effect of phytochemicals in *A. muricata* ripe fruit pulp showed better binding affinity for aldose reductase, afterwards alpha-amylase and alpha-glucosidase, through the interaction of epoxymurin-A, montecristin, and dicaffeoylquinic acid (Akinlolu et al., 2023). Therefore, the objective of this study is to computationally investigate *A. muricata's* fruit phytochemicals (such as acetogenins, alkaloids, cyclopeptides, and flavonoids), assessing their pharmacokinetics and binding dynamics with key molecular targets, contributing to the overall promotion of human well-being.

2. Materials and methods

2.1. Ligand preparation

The primary phytochemical constituents of *A. muricata* (L.) fruit were identified based on literature findings (Coria-Tellez et al., 2018), and their structures were retrieved from the NCBI PubChem Compound database (https://pubchem.ncbi.nlm.nih.gov/) in SMILES formats.

2.2. In silico Pharmacokinetics prediction

The *in silico* ADME (absorption, distribution, metabolism, and excretion) screening of the compounds was conducted using the SwissADME server (www.swissadme.ch), employing default parameters and the SMILES format (Daina et al., 2017).

2.3. In silico target prediction

The SMILES representation of each ligand facilitated target prediction analysis on the SEA Search Server (http://www.sea.bkslab.org/) (Keiser et al., 2007), with Homo sapiens selected as the target organism.

2.4. Protein-protein interaction analysis

To establish relationships among the predicted targets of *A. muricata* phytochemicals, target proteins underwent protein-protein interaction (PPI) profiling on the STRING webserver (https://string-db.org/, Szklarczyk et al., 2021).

2.5. Target gene network analyses

Predicted target gene IDs were compiled for network analyses, including transcription factor enrichment analysis, protein-protein interaction network expansion, and kinase enrichment analysis. This comprehensive analysis utilized the eXpression2Kinases (X2K) Web server (https://maayanlab.cloud/X2K/), with the human organism selected as the background reference (Clarke et al., 2018).

2.6. Molecular docking

The SMILES of the ligands underwent 3D structure optimization using ACDLab/Chemsketch software, saved in .mol format, and further converted to .pdb format using PyMol software. The 3D structure of c-Myc was obtained as AlphFold pdb format from UniProt database (UniProt ID: P01106). Both ligand and c-Myc target protein structures were formatted to pdbqt using AutoDock Tools (ADT) v1.5.6 (Morris et al., 2009). Ligand-protein docking was executed with AutoDock Vina v1.2.3 (Trott and Olson, 2010; Eberhardt et al., 2021), following established protocols (Fatoki et al., 2023). The resulting binding affinity and ligand-target interactions were analyzed and visualized using ezLigPlot on the ezCADD webserver (http://dxulab.org/software) (Tao et al., 2019).

2.7. Molecular dynamics simulation

Molecular dynamics simulations lasting 100 nanoseconds were conducted using Desmond, a Schrödinger LLC package (Bowers et al., 2006; Schrödinger, 2018; Fatoki et al., 2024). Initial protein and ligand complexes from the docking studies underwent preprocessing with Maestro's protein preparation wizard, including optimization and minimization. The systems were prepared using the System Builder tool, employing an orthorhombic TIP3P solvent model. The OPLS-2005 force field governed the simulation, with neutralization achieved by adding 0.15 M NaCl counter ions to mimic physiological conditions (Fatoki, 2022). The NPT ensemble with 310 K temperature and 1 atm pressure was selected, and models were relaxed before simulation. Trajectories were saved every 100 ps, and post-simulation analysis assessed for root-mean-square deviation (RMSD), root-mean-square fluctua-

tion (RMSF), and protein-ligand interaction profiles. Additionally, prime molecular mechanics/generalized Born surface area (MMGBSA) was used to evaluate binding free energy (Zhang et al., 2017; Schrödinger, 2019; Fatoki et al., 2024).

3. Results

The investigation into the phytoconstituents of *A. muricata* (L) revealed diverse pharmacokinetic characteristics. Table 1 illustrates that certain phytoconstituents exhibit low gastrointestinal absorption (GIA) due to insolubility, except for Annonaine, Asimilobine, Cinnamic acid, Coumaric acid, Fisetin, Kaempferol, Morin, Nornuciferine, and Reticuline, which are soluble and demonstrate high GIA. Additionally, Annonaine, Asimilobine, Cinnamic acid, Coumaric acid, N-methylcoclaurine, Nornuciferine, and Reticuline permeate the blood-brain barrier (BBB), while some compounds can inhibit specific cytochromes (CYPs) and act as substrates for P-glycoprotein (P-gp).

Table 2 presents the results of molecular target prediction, highlighting that *A. muricata* phytocompounds frequently target Programmed cell death protein 4 (PDCD4), followed by nuclear receptor subfamily 0 group B member 2 (NR0B2), Cytochrome P450 1B1 (CYP1B1), and others. Rankings are based on p-value and Maximum Tanimoto Coefficient (MTC), indicating similarity between compounds from reference and query targets.

The protein-protein interaction network of *A. muricata* molecular targets identifies Cytochrome P450 1B1 (CYP1B1) as a central protein linking metabolism to functional activity pathways. This is illustrated by key proteins such as tyrosinase (TYR), Tyrosine 3-monooxygenase (TH), interleukin 2 (IL2), Testosterone 17-beta-dehydrogenase 3 (HSD17B3), and others, as shown in Figure 1. Furthermore, the molecular target genes network of *A. muricata* bioactive compounds reveals signaling pathways involving kinases (e.g., MAPK3, MAPK14, CDK1, CDK2, GSK3B, ERK1, ERK2, CSNK2A1, CLK2, CHEK2, PRKDC, BUB1B) and transcription factors (e.g., PPARG, STAT3, FOS, TRIM28, EZH2, TCF3, REST, ZBTB44, ZNF529, NANOG), as depicted in Figures 2 and 3.

Table 3 displays the molecular docking results of *A. muricata* phytochemicals with the highly targeted protein PDCD4. Luteolin 3,7-di-O-glucoside exhibited the highest binding affinity for PDCD4 (−7.65 kcal.mol^{-1}), followed by Annonaine (−7.294 kcal.mol^{-1}) and Dihydrokaempferol-hexoside (−7.012 kcal.mol^{-1}). In comparison, the standard compound Dexamethasone showed a binding affinity of −6.682 kcal.mol^{-1}. Figure 4 illustrates the binding pose of the complex with high binding affinity, highlighting the involved amino acid residues.

MDS was employed to assess the structural stability of both the protein and the binding status of the ligand in a physiologically relevant environment. The outcomes of the MDS studies, using the PDCD4-Annonaine and PDCD4-Dexamethasone binding complexes, are presented in Figure 5, providing valuable insights into the dynamic behavior and interactions of the protein-ligand complexes under realistic conditions.

For the Annonaine - PDCD4 complex, RMSD analysis indicated an RMSD of 18.0 Å for the protein and 16 Å for the ligand over the 0–100 ns period (Figure 5a). RMSF of PDCD4 showed maximal fluctuation at amino acid residues 100–150 and C-terminal (Figure 5b). Protein-ligand interactions revealed details about the involved amino acid residues in hydrophobic interactions, hydrogen bonds, water bridges, and ionic interactions, including GLU161, PHE164, GLU165, and LYS242 (Figure 5c). For the Dexamethasone - PDCD4 complex, RMSD analysis indicated an RMSD of 21 Å for the protein and 12.5 Å for the ligand over the 0–100 ns period (Figure 5d). RMSF of PDCD4 showed maximal fluctuation at amino acid residues 100–150 and N-terminal (Figure 5e). Protein-ligand interactions revealed details about the involved amino acid residues in hydrophobic interactions, hydrogen bonds, water bridges, and ionic interactions, including GLU165, GLU195, SER198, and LYS238 (Figure 5f).

A schematic of detailed ligand atom interactions with the protein residues is presented in Figure 6, validating the amino acid residues involved in the docking interactions. The computed binding free energies using MMGBSA are presented in Table 4, providing insights into the stability and energetics of the protein-ligand interactions throughout the simulation. Notably, the Annonaine - PDCD4 complex at 0ns and 100ns exhibited a binding energy of −35.851 kcal.mol^{-1} and −39.019 kcal.mol^{-1} respectively, while the Dexamethasone - PDCD4 complex at 0ns and 100ns displayed a binding energy of −28.489 and −28.284 kcal.mol^{-1} respectively. Thus, the stability of the two complexes were maintained during the simulation.

4. Discussion

A. muricata, a noteworthy member of the Annonaceae family, exhibits diverse pharmacological properties. This study computationally evaluated the phytoconstituents of *A. muricata* for pharmacokinetic properties, molecular targets, gene signaling pathway kinases, transcription factors, binding affinity, and stability with PDCD4.

According to Mutakin et al. (2022), the major compounds and secondary metabolites are present in the *A. muricata* plant are acetogenins, flavonoids, alkaloids, essential oils, carotenoids, vitamins, and cyclopeptides; and that its pharmacological properties included wound healing properties (4%), antihypertensive (6%), antiviral (8%), antibacterial (8%), antidiarrhea (8%), antiprotozoal (10%), antidiabetic (14%), antiulcer (17%), and anticancer (25%). Also, previous studies have reported cytotoxic effect of annonacin, annonacin-10-one cis-annoreticuin, and corossolone; whereas kaempferol, montecristin, luteolin 3,7-di-o-glucoside, kaempferol 3-o-rutinoside, and morin possessed antioxidant properties (Coria-Tellez et al., 2018; Akinlolu et al., 2023)

The pharmacokinetics assessment unveiled that most phytoconstituents possess moderate solubility and intestinal absorption, with some capable of permeating the blood-brain barrier (BBB). Moreover, insolubility of some phytochemicals especially phenolic compounds, could be modified by their interactions within the food product matrix to form soluble complexes and conjugates, that increase absorption rate, reduce first-pass metabolism and subsequent increase bioavailability. Notably, Annonaine demonstrated favorable gastrointestinal absorption (GIA), potentially attributed to its large molecular size without predicted inhibitory effects on cytochromes (CYPs). Conversely, quercetin displayed high GIA, likely due to its moderate molecular size and some inhibitory effects on specific CYPs. GIA plays a pivotal role in drug efficacy, influencing the bioavailability of administered doses. Alterations in CYP activity can impact drug metabolism, affecting bioavailability or efficacy (Martin et al., 2013). Molecular size, expressed in terms of molecular weight and volume, serves as crucial toxicity metrics influencing compound bioavailability and toxicity (Kostal, 2016). The toxicity of drug decreases as the lipophilicity (Log P value) decreases, because the higher the lipophilicity the lesser the solubility. Log P value around 2.2 are considered more suitable for

Table 1. Predicted pharmacokinetics properties of selected ligands

SN	Ligands	Predicted ADME Parameter from SWISSADME												
		MW	MR	TPSA (Å²)	Log P	ESOL Log S	ESOL Class	GIA	BBB permeant	P-gp	CYPs inhibitor	Lip	BS	SA
1	Annonacin	596.88	172.67	116.45	6.92	−7.13	Poorly soluble	Low	No	No	CYP3A4	1	0.55	7.36
2	Annonacin-10-one	594.86	171.71	113.29	6.83	−6.8	Poorly soluble	Low	No	Yes	CYP3A4	1	0.55	7.18
3	Annonaine	265.31	80.13	30.49	2.88	−3.71	Soluble	High	Yes	Yes	CYP1A2, CYP2D6, CYP3A4	0	0.55	3.36
4	Cis-Annoreticuin	596.88	172.67	116.45	6.94	−7.13	Poorly soluble	Low	No	No	CYP3A4	1	0.55	7.36
5	Asimilobine	267.32	82.59	41.49	2.65	−3.54	Soluble	High	Yes	Yes	CYP1A2, CYP2D6, CYP3A4	0	0.55	3.24
6	Cinnamic acid	148.16	43.11	37.3	1.79	−2.37	Soluble	High	Yes	No	NONE	0	0.85	1.67
7	Corossolone	578.86	170.55	93.06	7.75	−7.66	Poorly soluble	Low	No	Yes	NONE	2	0.17	6.9
8	Coumaric acid	164.16	45.13	57.53	1.26	−2.02	Soluble	High	Yes	No	NONE	0	0.85	1.61
9	Dicaffeoylquinic acid	516.45	126.9	211.28	0.91	−3.65	Soluble	Low	No	Yes	NONE	3	0.11	4.83
10	Dihydrokaempferol-hexoside	450.39	105.12	186.37	−0.5	−2.8	Soluble	Low	No	Yes	NONE	2	0.17	5.24
11	Epoxymurin-A	530.86	167.55	38.83		−10.03	Insoluble	Low	No	Yes	NONE	2	0.17	6.47
12	Epoxymurin-B	530.86	167.55	38.83		−10.03	Insoluble	Low	No	Yes	NONE	2	0.17	6.47
13	Epomusenin-A	558.92	177.17	38.83		−10.75	Insoluble	Low	No	Yes	NONE	2	0.17	6.73
14	Epomusenin-B	558.92	177.17	38.83		−10.75	Insoluble	Low	No	Yes	NONE	2	0.17	6.73
15	Fisetin	286.24	76.01	111.13	1.55	−3.35	Soluble	High	No	No	CYP1A2, CYP2D6, CYP3A4	0	0.55	3.16
16	Kaempferol	286.24	76.01	111.13	1.58	−3.31	Soluble	High	No	No	CYP1A2, CYP2D6, CYP3A4	0	0.55	3.14
17	Kaempferol 3-O-rutinoside	594.52	139.36	249.2		−3.42	Soluble	Low	No	Yes	NONE	3	0.17	6.48
18	Luteolin 3,7-di-O-glucoside	610.52	140.26	269.43		−3.22	Soluble	Low	No	Yes	NONE	3	0.17	6.39
19	Montecristin	574.92	180.05	66.76	9.92	−9.64	Poorly soluble	Low	No	Yes	NONE	2	0.17	6.82
20	Morin	302.24	78.03	131.36	1.2	−3.16	Soluble	High	No	No	CYP1A2, CYP2D6, CYP3A4	0	0.55	3.25
21	Muricatetrocin B	470.64	129.41	116.45	3.8	−4.1	Moderately soluble	High	No	No	CYP3A4	0	0.55	6.21
22	Muricatocin A	612.88	173.84	136.68	6.17	−6.61	Poorly soluble	Low	No	No	CYP3A4	1	0.55	7.5
23	Myricetin	318.24	80.06	151.59	0.79	−3.01	Soluble	Low	No	No	CYP1A2, CYP3A4	1	0.55	3.27
24	N-methylcoclaurine	299.36	90.52	52.93	2.59	−3.82	Soluble	High	Yes	Yes	CYP2D6	0	0.55	2.92
25	Nornuciferine	281.35	87.06	30.49	3.01	−3.74	Soluble	High	Yes	Yes	CYP1A2, CYP2D6, CYP3A4	0	0.55	3.35
26	Reticuline	329.39	97.01	62.16	2.6	−3.88	Soluble	High	Yes	Yes	CYP2D6	0	0.55	3.07
27	Sabadelin	530.86	167.55	38.83		−10.03	Insoluble	Low	No	Yes	NONE	2	0.17	6.47
28	Xylomatenin	622.92	181.81	116.45	7.47	−7.43	Poorly soluble	Low	No	No	CYP3A4	1	0.55	7.58

Physicochemical properties: Molecular weight (MW), Molar Refractivity (MR), Total polar surface area (TPSA). Lipophilicity: Consensus Log P. Water Solubility: ESOL Log S, ESOL Class. Pharmacokinetics: Gastrointestinal absorption (GIA), Blood-brain barrier (BBB), P-glycoprotein (P-gp) substrate, Inhibition of Cytochrome P450 (CYPs) type CYP1A2, CYP2C19, CYP2C9, CYP2D6, and CYP3A4. Druglikeness: Lipinski (Lip), Bioavailability Score (BS), Medicinal Chemistry: Synthetic accessibility (SA).

Table 2. Target prediction results

SN	Compound	Target gene code	Target description	p-value	MTC
1	Annonacin	PDCD4	Programmed cell death protein 4	4.236e-74	0.36
		PTGER2	Prostaglandin E2 receptor EP2 subtype	1.586e-06	0.32
2	Annonacin-10-one	PDCD4	Programmed cell death protein 4	6.804e-70	0.33
		IL6ST	Interleukin-6 receptor subunit beta	4.887e-23	0.30
		PPM1A	Protein phosphatase 1A	7.318e-23	0.28
		SLCO2A1	Solute carrier organic anion transporter family member 2A1	8.104e-18	0.28
3	Annonaine	TAS1R1	Taste receptor type 1 member 1	3.462e-06	0.29
4	Cis-Annoreticuin	PDCD4	Programmed cell death protein 4	4.236e-74	0.36
5	Asimilobine	TH	Tyrosine 3-monooxygenase	1.001e-39	0.32
		DRD1	D(1A) dopamine receptor	1.11e-16	0.39
		MMP26	Matrix metalloproteinase-26	1.384e-07	0.32
6	Cinnamic acid	HCAR2	Hydroxycarboxylic acid receptor 2	8.423e-10	1.00
		NR0B2	Nuclear receptor subfamily 0 group B member 2	9.432e-46	0.31
		GPR183	G-protein coupled receptor 183	2.941e-42	0.39
		SENP2	Sentrin-specific protease 2	3.568e-41	0.33
		CYP1B1	Cytochrome P450 1B1	6.792e-40	0.48
		RCOR3	REST corepressor 3	1.157e-39	0.31
		PAM	Peptidyl-glycine alpha-amidating monooxygenase	1.372e-38	0.52
		CHRNA10	Neuronal acetylcholine receptor subunit alpha-10	1.097e-35	0.28
7	Corossolone	PDCD4	Programmed cell death protein 4	3.7e-33	0.30
		PPM1A	Protein phosphatase 1A	2.063e-23	0.29
8	Coumaric acid	CA3	Carbonic anhydrase 3	1.966e-29	1.00
		CA6	Carbonic anhydrase 6	4.201e-29	1.00
		CA5B	Carbonic anhydrase 5B, mitochondrial	5.523e-27	1.00
		CA5A	Carbonic anhydrase 5A, mitochondrial	2.466e-26	1.00
		CA14	Carbonic anhydrase 14	7.845e-21	1.00
		CA7	Carbonic anhydrase 7	9.975e-20	1.00
		AKR1B1	Aldo-keto reductase family 1 member B1	5.551e-16	1.00
9	Dicaffeoylquinic acid	NSD2	Histone-lysine N-methyltransferase NSD2	0.0008982	1.00
		CXCL12	Stromal cell-derived factor 1	1.437e-76	0.38
		NR0B2	Nuclear receptor subfamily 0 group B member 2	3.814e-47	0.33
		MYOC	Myocilin	1.277e-31	0.39
10	Dihydrokaempferol-hexoside	TOP1	DNA topoisomerase 1	6.893e-61	0.36
		SLC5A2	Sodium/glucose cotransporter 2	8.932e-58	0.43
		SLC28A3	Solute carrier family 28 member 3	9.656e-53	0.42
		TYR	Tyrosinase	5.641e-36	0.42
		IL2	Interleukin-2	5.276e-30	0.40
		CBS	Cystathionine beta-synthase	2.038e-27	0.48
11	Epoxymurin-A	PDCD4	Programmed cell death protein 4	1.016e-45	0.36
		LYPLA2	Acyl-protein thioesterase 2	1.4e-22	0.29

Table 2. Target prediction results - *(continued)*

SN	Compound	Target gene code	Target description	p-value	MTC
12	Epoxymurin-B	PDCD4	Programmed cell death protein 4	1.016e-45	0.36
		LYPLA2	Acyl-protein thioesterase 2	1.4e-22	0.29
13	Epomusenin-A	PDCD4	Programmed cell death protein 4	1.016e-45	0.36
		LYPLA2	Acyl-protein thioesterase 2	1.4e-22	0.29
14	Epomusenin-B	PDCD4	Programmed cell death protein 4	1.016e-45	0.36
		LYPLA2	Acyl-protein thioesterase 2	1.4e-22	0.29
15	Fisetin	ELAVL3	ELAV-like protein 3	2.048e-65	0.66
		HSD17B3	Testosterone 17-beta-dehydrogenase 3	1.047e-52	0.43
		ALDH2	Aldehyde dehydrogenase, mitochondrial	4.45e-50	0.41
		CYP1B1	Cytochrome P450 1B1	6.994e-39	0.66
16	Kaempferol	ELAVL3	ELAV-like protein 3	1.407e-81	0.78
		PTPRS	Receptor-type tyrosine-protein phosphatase S	5.492e-59	0.75
		CBS	Cystathionine beta-synthase	9.017e-51	0.45
		CREB1	Cyclic AMP-responsive element-binding protein 1	5.513e-45	0.30
		P4HB	Protein disulfide-isomerase	6.101e-41	0.52
17	Kaempferol 3-O-rutinoside	P4HB	Protein disulfide-isomerase	3.535e-71	1.00
		SLC28A3	Solute carrier family 28 member 3	1.353e-43	0.35
		ELAVL3	ELAV-like protein 3	2.773e-43	0.39
		IL2	Interleukin-2	1.262e-31	0.42
		TYR	Tyrosinase	9.763e-30	0.34
		XDH	Xanthine dehydrogenase/oxidase	1.157e-25	0.65
18	Luteolin 3,7-di-O-glucoside	CREB1	Cyclic AMP-responsive element-binding protein 1	5.266e-69	0.35
		SLC5A2	Sodium/glucose cotransporter 2	3.962e-60	0.41
		SLC28A3	Solute carrier family 28 member 3	3.077e-50	0.40
		IL2	Interleukin-2	5.836e-40	0.89
19	Montecristin	PDCD4	Programmed cell death protein 4	1.128e-77	0.41
		SLCO2A1	Solute carrier organic anion transporter family member 2A1	2.172e-38	0.32
		POLH	DNA polymerase eta	3.331e-16	0.31
20	Morin	PTPRS	Receptor-type tyrosine-protein phosphatase S	6.131e-56	1.00
		MPG	DNA-3-methyladenine glycosylase	1.089e-50	1.00
		DAPK1	Death-associated protein kinase 1	1.344e-21	1.00
		ELAVL3	ELAV-like protein 3	8.402e-82	0.68
		P4HB	Protein disulfide-isomerase	3.742e-36	0.44
21	Muricatetrocin B	PDCD4	Programmed cell death protein 4	2.688e-59	0.33
22	Muricatocin A	PDCD4	Programmed cell death protein 4	1.009e-81	0.40
23	Myricetin	ELAVL3	ELAV-like protein 3	2.196e-101	1.00
		XDH	Xanthine dehydrogenase/oxidase	5.844e-36	1.00
24	N-methylcoclaurine	DRD1	D(1A) dopamine receptor	1.982e-95	0.58
		DHCR7	7-dehydrocholesterol reductase	2.187e-43	0.50
		TUBB1	Tubulin beta-1 chain	5.991e-26	0.35

Table 2. Target prediction results - *(continued)*

SN	Compound	Target gene code	Target description	p-value	MTC
		ABCB1	ATP-dependent translocase ABCB1	9.037e-26	0.45
		SLC18A2	Synaptic vesicular amine transporter	4.29e-24	0.35
25	Nornuciferine	TUBB	Tubulin beta chain	4.386e-25	0.31
26	Reticuline	DRD1	D(1A) dopamine receptor	9.256e-98	0.56
		DHCR7	7-dehydrocholesterol reductase	3.993e-44	0.51
		TUBB1	Tubulin beta-1 chain	1.432e-43	0.40
		FSHR	Follicle-stimulating hormone receptor	1.151e-29	0.30
		NDUFA1	NADH dehydrogenase [ubiquinone] 1 alpha subcomplex subunit 1	5.531e-17	0.32
27	Sabadelin	PDCD4	Programmed cell death protein 4	1.016e-45	0.36
		LYPLA2	Acyl-protein thioesterase 2	1.4e-22	0.29
28	Xylomatenin	PDCD4	Programmed cell death protein 4	9.378e-70	0.41
		SLCO2A1	Solute carrier organic anion transporter family member 2A1	1.494e-36	0.31

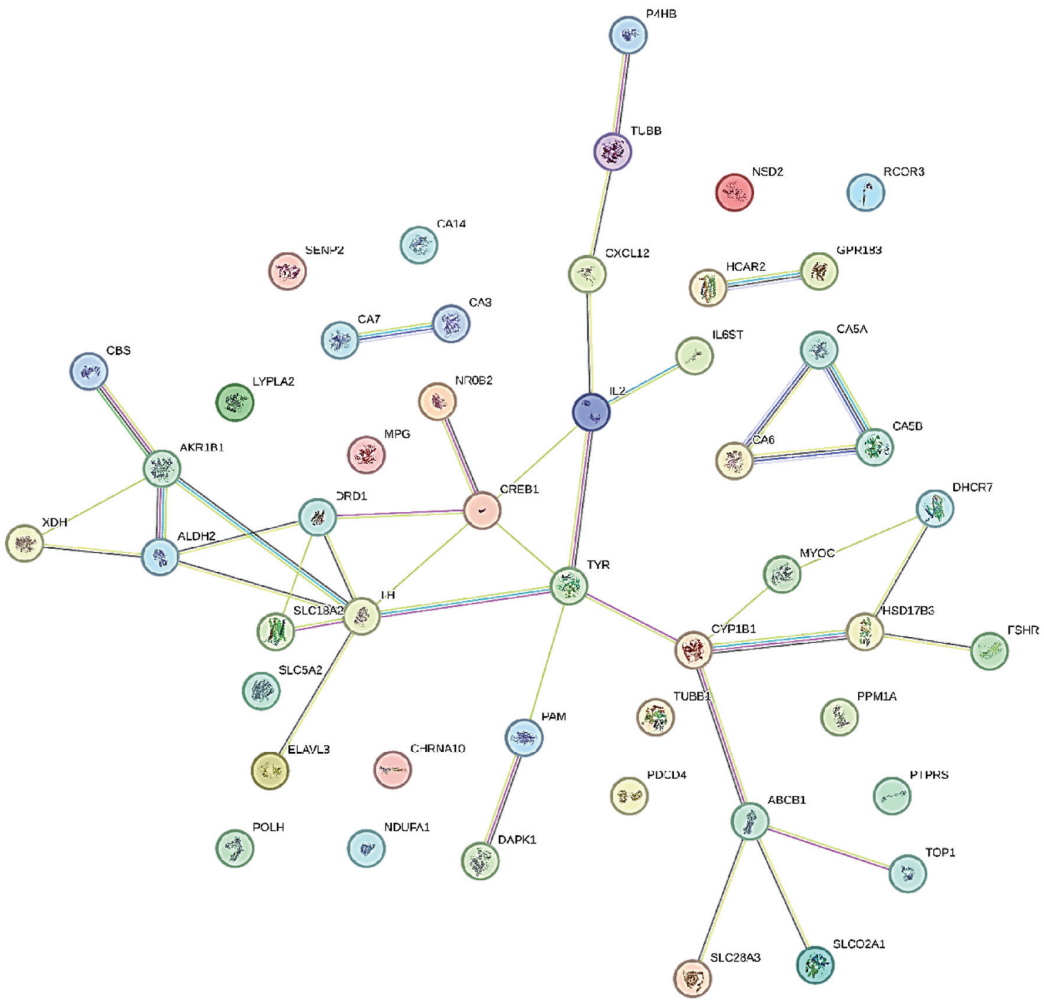

Figure 1. Protein-protein interaction of *A. muricata* molecular targets.

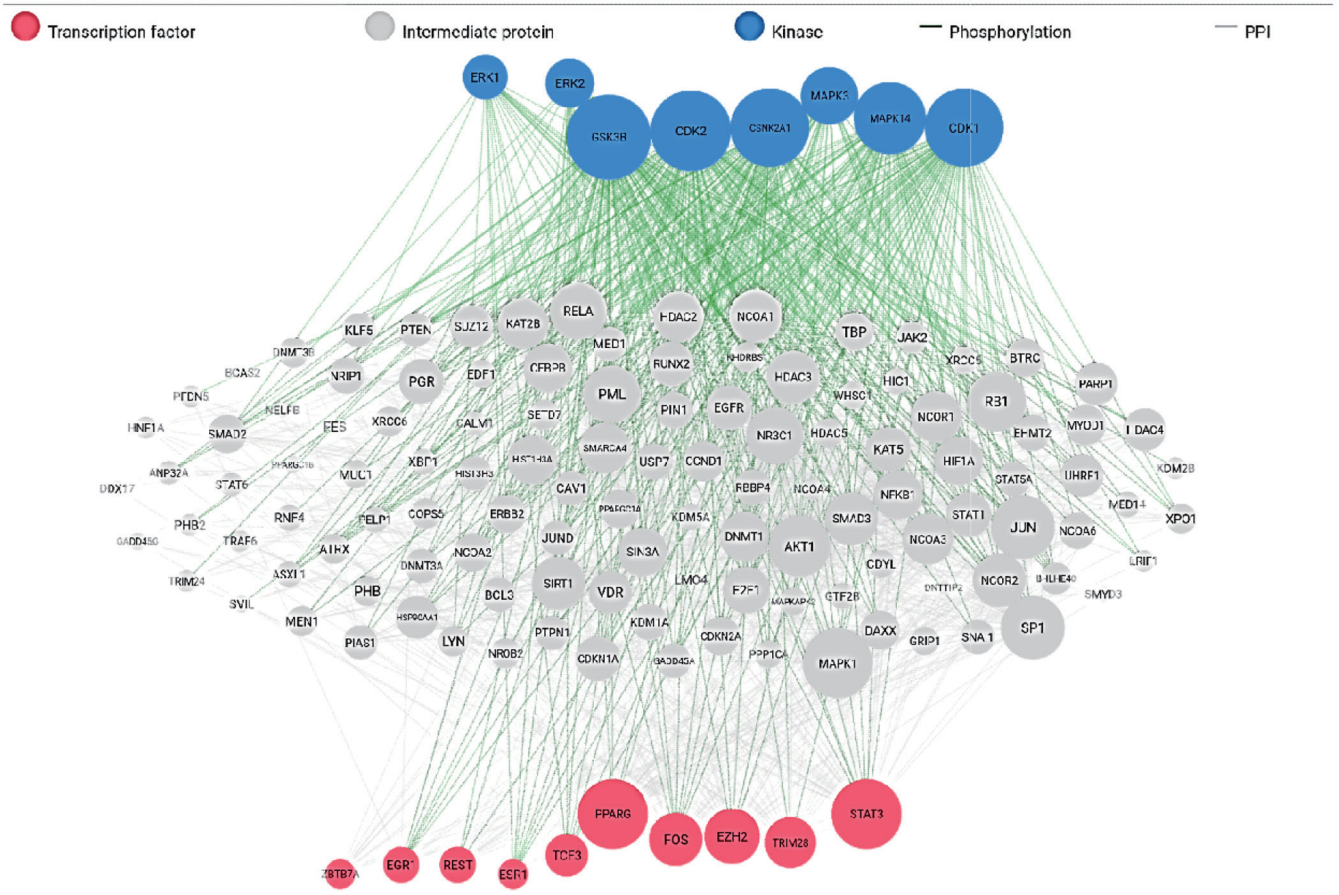

Figure 2. Overall molecular target genes network.

oral bioavailability (Arnott and Planey, 2012).

The number of hydrogen-bond donors and acceptors serves as fundamental molecular descriptors predicting the oral bioavailability of small drug candidates, while the number of heavy atoms, combined with binding affinity from docking, determines ligand efficiency (Ibraheem et al., 2019). Generally, hydrogen-bond donors and acceptors are presumed to impact passive diffusion across cell membranes, a critical event in drug absorption and distribu-

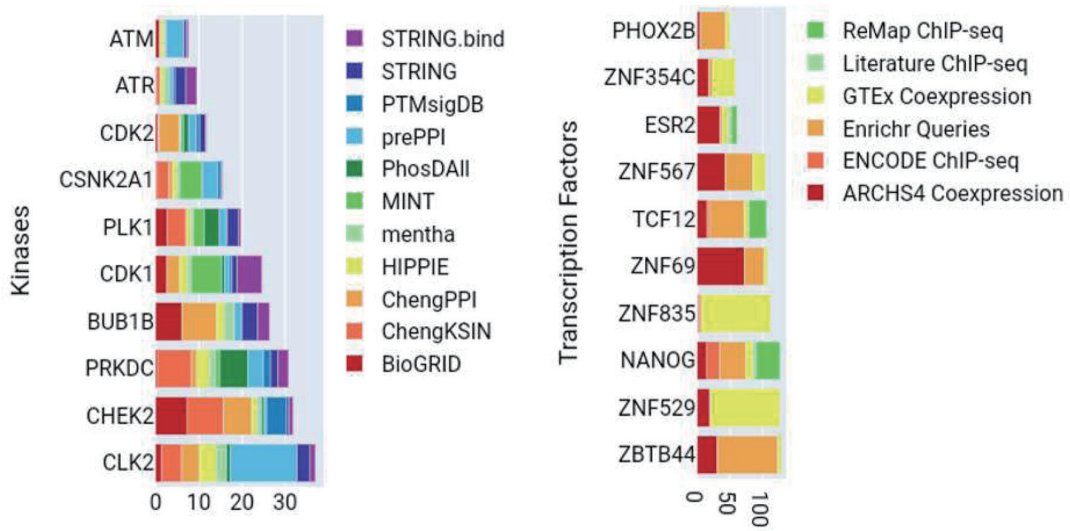

Figure 3. Average rank of kinases and transcription factors across all the library.

Table 3. Molecular docking results

S.N	Phytochemicals	PubChem CID	PDCD4 (AlphaFold ID: AF-Q53EL6) Binding Affinity ΔG (kcal.mol^{-1})
1	Annonacin	354398	−4.741
2	Annonacin-10-one	180161	−4.591
3	Annonaine	160597	−7.294
4	Cis-Annoreticuin	72778911	−4.869
5	Asimilobine	160875	−6.409
6	Cinnamic acid	444539	−3.96
7	Corossolone	4366126	−4.615
8	Coumaric acid	637542	−5.183
9	Dicaffeoylquinic acid	12358846	−6.775
10	Dihydrokaempferol-hexoside	10478918	−7.012
11	Epoxymurin-A	5281161	−4.416
12	Epoxymurin-B	131752983	−3.789
13	Epomusenin-A	10507050	−3.842
14	Epomusenin-B	10698082	−3.614
15	Fisetin	5281614	−6.979
16	Kaempferol	5280863	−6.749
17	Kaempferol 3-O-rutinoside	5318767	−6.629
18	Luteolin 3,7-di-O-glucoside	5490298	−7.65
19	Montecristin	102083640	−3.861
20	Morin	5281670	−6.884
21	Muricatetrocin B	393472	−5.362
22	Muricatocin A	133072	−5.191
23	Myricetin	5281672	−6.538
24	N-methylcoclaurine	440595	−5.946
25	Nornuciferine	41169	−6.226
26	Reticuline	439653	−5.907
27	Sabadelin	101006011	−3.426
28	Xylomatenin	10484035	−4.5
STD	Dexamethasone	5743	−6.682

Docking parameter: PDCD4 [spacing: 0.525, box size: 126 × 126 × 126, center: −9.248 × 0.161 × 1.314].

tion (Coimbra et al., 2021). P-glycoprotein (P-gp), a membrane transporter, actively pumps drugs out of cells, influencing drug bioavailability. The interplay of gastrointestinal absorption (GIA), blood-brain barrier (BBB) penetration, P-gp modulation, and cytochrome inhibition collectively shapes the pharmacokinetics and pharmacodynamics of phytochemicals or bioactive compounds.

Target prediction revealed that human programmed cell death 4 (PDCD4) is possibly the most frequent protein modulated by *A. muricata* phytochemicals. However, those targeting PDCD4 were found to be poorly soluble or insoluble, exhibit low GIA, and were not BBB permeants. PDCD4, an apoptosis-associated gene, is regulated by interleukins IL-2, IL-12, and IL-15, and functions as a tumor suppressor gene, playing essential roles in apoptosis, protein translation, signal transduction, and inflammation mediator stimulation (Zhang et al., 2014; Pin et al., 2020). Loss or downregulation of PDCD4 expression promotes tumor cell proliferation, invasion, and metastasis while reducing tumor cell apoptosis in various cancer types (Wang et al., 2019). PDCD4 downregulation is associated with chemoresistance, coinciding with a reduction in eukaryotic initiation factor-4A (eIF4A) interaction (González-Ortiz et al., 2022). Notably, cryptotanshinone, a natural terpene, has been reported to potentially upregulate eIF4A, suggesting a potential increase in PDCD4 expression (Galindo-Hernandez et al., 2019; González-Ortiz et al., 2022). Thus, *A. muricata* phytochemicals could be extrapolated with the same effect on PDCD4 directly or indirectly, because activation but not inhibition of PDCD4 expression could account for anticancer properties of *A. muricata.*

Numerous studies have demonstrated that PDCD4 overexpres-

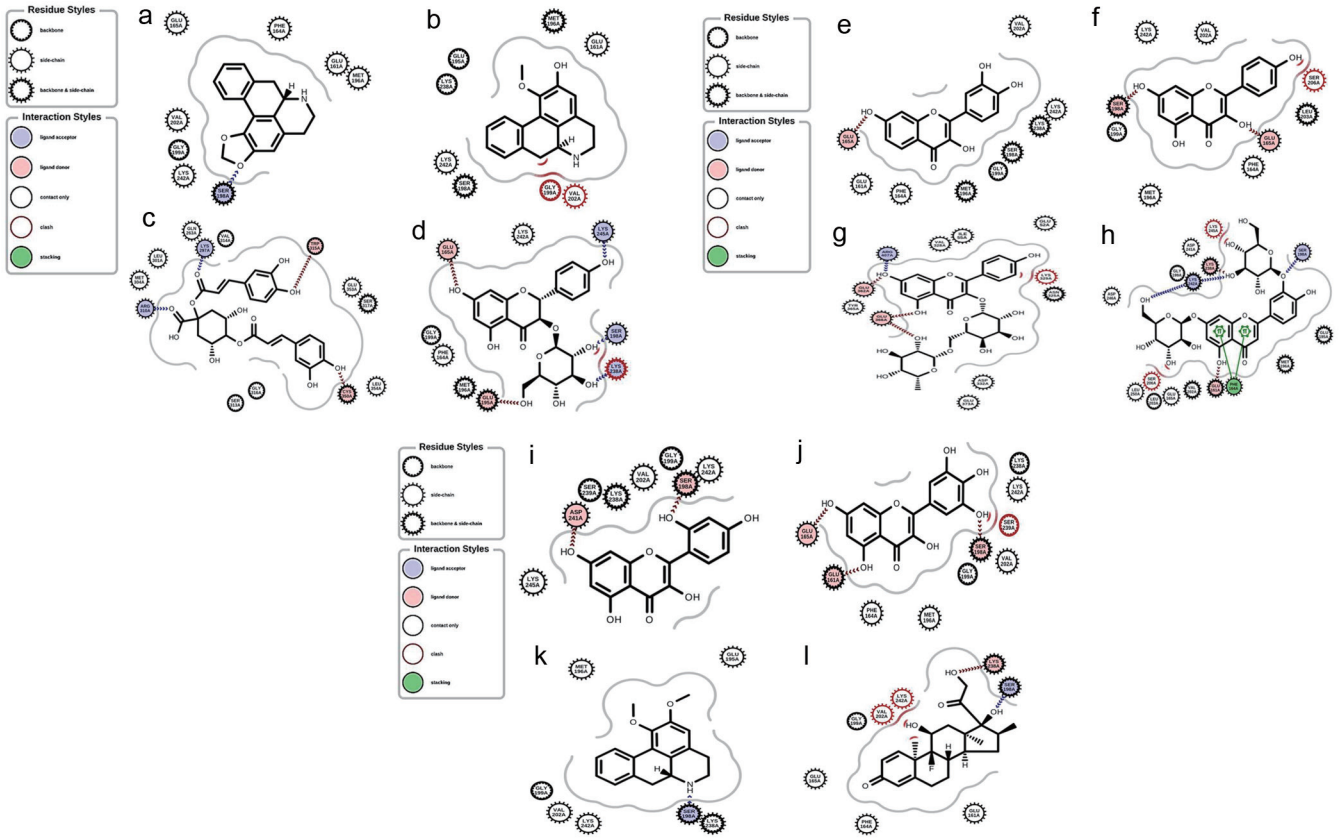

Figure 4. Interaction of the binding poses of PDCD4 with: (a) Annonaine; (b) Asimilobine; (c) Dicaffeoylquinic acid; (d) Dihydrokaempferol-hexoside; (e) fisetin; (f) Kaempferol; (g) Kaempferol-3-O-rutinoside; (h) Luteolin-3,7-di-O-glucoside; (i) Morin; (j) Myricetin; (k) Nornuciferine; (l) Dexamethasone.

sion significantly enhances the chemosensitivity of various cancer cells, including acute myeloid leukemia, breast cancer, ovarian cancer, non-small cell lung cancer (NSCLC), rectal cancer, and pancreatic cancer, to chemotherapy drugs like dexamethasone and taxol (Shibahara et al., 1995; Wang et al., 2019). PDCD4 overexpression in lung tumor cells has been linked to the suppression of the transcriptional activation of Nrf2 through its negative regulator, Keap1 (Hwang et al., 2020).

This study predicted several kinases involved in the mechanism of action of *A. muricata* phytochemicals. The implicated signaling pathways connecting many of these kinases and transcription factors include MAPK, PI3K/Akt, and JAK/STAT3 pathways, crucial for cell survival, proliferation, and apoptosis. These findings align with previous report that inhibition of STAT3 pathway led to the downregulation of MicroRNA-21 and upregulation of PDCD4 (Asangani et al., 2008; Singh et al., 2015). Additionally, AKT2, among the AKT isoforms, has been reported to interact with PDCD4, suppressing PDCD4 in glioma cells. PDCD4 regulates the expression of IL-5, CCL-5, VEGF, and CXCL10 via the NF-kB pathway. Depletion of PDCD4 levels promotes angiogenic activity of glioma cells through the VEGF-STAT3 pathway (Pin et al., 2020). PDCD4 inhibits NF-κB signaling to reduce NF-κB-dependent matrix metallopeptidase (MMP-9) expression in cancer cells, impacting tumor cell migration and apoptosis (Parks et al., 2004; Mao et al., 2017). A study by Drishya et al. (2020) reported that transcription factors RECK and TIMP-2 mediate the inhibition of MMP-2 and MMP-9 by *A. muricata*. Reduced PDCD4 expression promotes cell growth through the PI3K/Akt signaling pathway in NSCLC (Zhen et al., 2016). Furthermore, upregulation of PDCD4 suppresses the expression of the cell cycle regulatory molecule, cyclin-dependent kinase 4 (CDK4), while downregulation of PDCD4 enhances CDK4 expression (Jin et al., 2006; Hwang et al., 2010).

Molecular docking, a computational technique, predicts ligand binding sites and affinities on receptor surfaces. It involves generating numerous ligands poses on the receptor surface and scoring their predicted binding affinities (Rentzsch and Renard, 2015). The results of molecular docking studies revealed that only two compounds, Muricatetrocin B (−5.362 kcal.mol^{-1}) and Muricatocin A (−5.191 kcal.mol^{-1}), among the 13 compounds targeting PDCD4, exhibited good binding affinity. A binding affinity score of ≤−5.00 kcal.mol^{-1} indicates a strong affinity between the target protein and the ligand (Wong et al., 2022). Also, aromatic pi-pi interactions of the ligands with amino acid residues such as tryptophan, tyrosine, histidine, and phenylalanine within the target proteins, are very essential in drug design because it promotes molecular recognition and interactions, improve specificity and efficacy (Apeh et al., 2023).

Molecular dynamics simulation (MDS) was employed to assess atomic-level variations in the protein-ligand system and evaluate the stability of the protein-ligand complex in a dynamic environment (Fatoki, 2023). MD simulations track the evolution of cartesian coordinates for every atom in a system using a general physics model governing particle interaction (McCammon and Karplus, 2002). RMSD and Rg are utilized for assessing flexibility, compactness, and conformational divergence of protein struc-

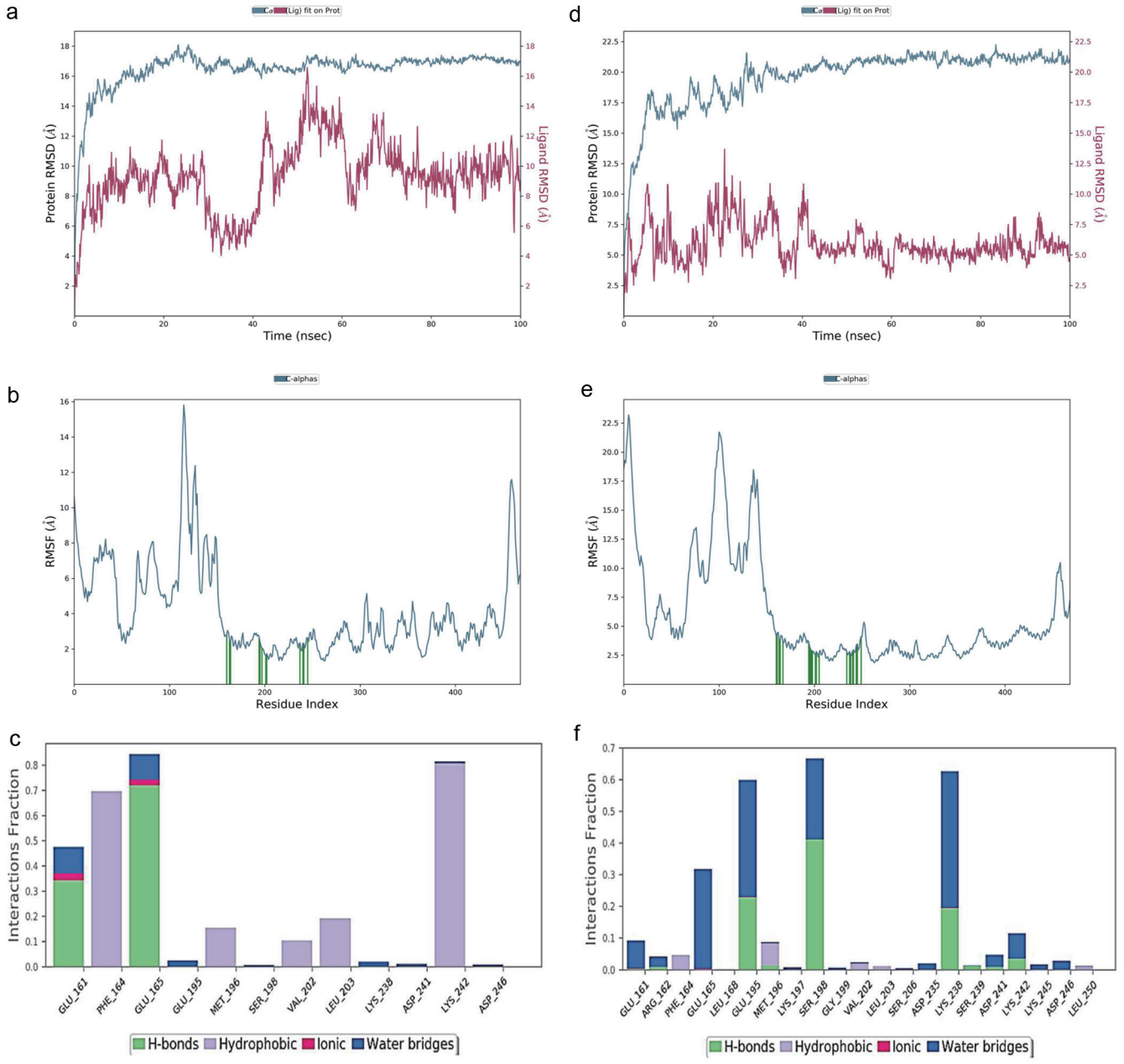

Figure 5. Protein-ligand complex simulation results (a) RMSD of Annonaine and PDCD4 (b) RMSF of PDCD4 on binding to Orientin. (c) Interaction profile of the contact between Annonaine and PDCD4 (d) RMSD of Dexamethasone and PDCD4. (e) RMSF of PDCD4 on binding to Quercetin; (f) Interaction profile of the contact between Dexamethasone and PDCD4.

tural ensembles. RMSD values less than 4 Å indicate relatively small conformational changes, suggesting stability during simulation (Fatoki et al., 2023). Protein-ligand interactions (or contacts) showed the contribution of amino acid residues in terms of hydrogen bonds, hydrophobic, ionic and water bridges, during the simulation, and could be used to elaborate the RMSF of the protein. The protein-ligand interactions stacked bar charts are normalized over the course of the trajectory; for instance, a value of 0.7 suggests that 70% of the simulation time the specific interaction was maintained. Prime MM-GBSA provides various energy properties, reporting energies for ligand, receptor, and complex structures, along with energy differences related to strain and binding (Fatoki, 2023). The total binding free energy confirms the stability of the complexes under physiological conditions.

5. Conclusion

Natural molecules emerge as promising candidates in drug development, offering numerous advantages and minimal side effects. The extract from *A. muricata* or its specific phytochemicals presents potential implications in drug discovery for conditions

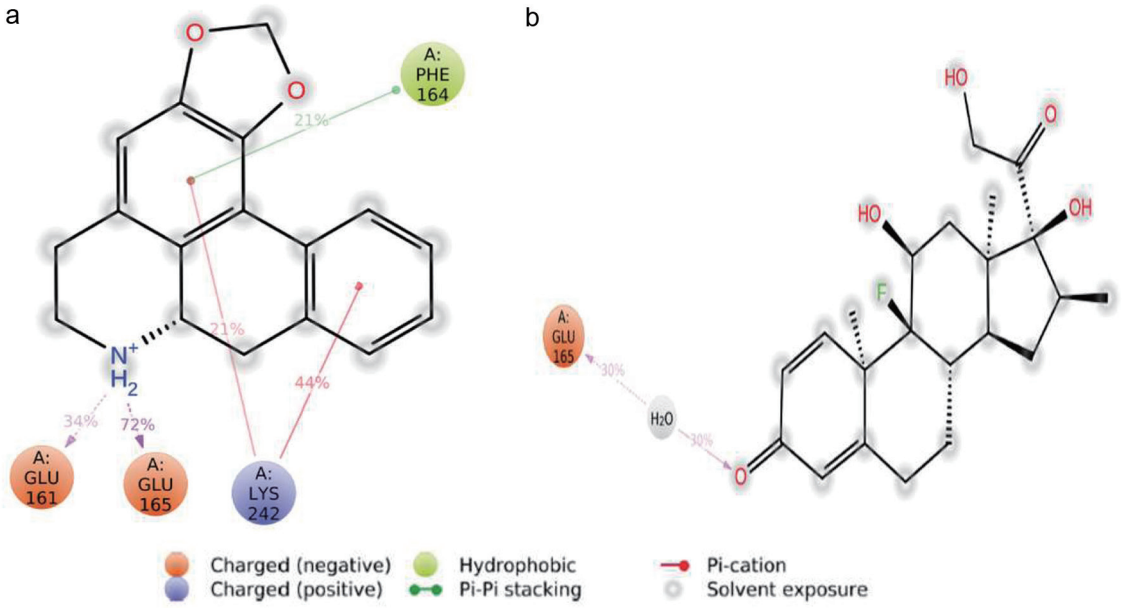

Figure 6. A schematic of detailed ligand-protein interactions (a) Annonaine and PDCD4 (b) Dexamethasone and PDCD4.

Table 4. Prime MMGBSA binding energy of interaction of PDCD4 with Annonaine and Dexamethasone respectively, before and after molecular dynamics simulation.

Complex	Simulation Time (ns)	MMGBSA ΔG^{bind} (kcal.mol^{-1})							
		Coulomb	Covalent	Hbond	Lipo	Packing	Solv_GB	vdW	G^{bind} (Total)
Annonaine and PDCD4	0	−64.428	2.791	−0.60	−14.323	−0.541	69.403	−28.149	−35.851
	100	−52.471	1.676	−0.797	−15.184	−1.519	52.998	−23.720	−39.019
Dexamethasone and PDCD4	0	0.913	0.092	−0.420	−7.605	0	11.380	−32.850	−28.489
	100	−4.693	−0.012	−0.027	−8.555	0	15.696	−30.694	−28.284

Covalent: Covalent binding energy; Coulomb: Coulomb energy; Lipo: Lipophilic energy; Hbond: Hydrogen bonding energy; Packing: Pi-pi packing correction; Solv GB: Generalized Born electrostatic solvation energy; vdW: Van der Waals energy; Total: Total energy (Prime energy).

like cancer and neurodegenerative diseases, operating through a mechanism of action that targets PDCD4. This study pioneers the notion that the anticancer properties of *A. muricata* may be attributed to PDCD4 overexpression, influencing the CDK/Akt/STAT3 pathway. Future research should delve into in vivo gene expression studies to evaluate the therapeutic efficacy of *A. muricata* extract or its specific phytochemicals, Muricatocin A and Muricatetrocin B, across various cancer types.

References

Abdullah, M., Syam, A.F., Meilany, S., Laksono, B., Prabu, O.G., Bekti, H.S., Indrawati, L., and Makmun, D. (2017). The Value of Caspase-3 after the Application of *Annona muricata* Leaf Extract in COLO-205 Colorectal Cancer Cell Line. Gastroenterol. Res. Pract. 2017: 165.

Ajiboye, B.O., Akinnusi, P.A., Fatoki, T.H., Adigun, D.K., Adewole, Z.O., Efekemo, E.O., Ayotunde, B.T., Julius, B.P., Falode, J.A., Ajuwon, O.R., and Oyinloye, B.E. (2023). *In silico* assessment of *Hibiscus sabdariffa* as a possible therapeutic agent for breast cancer management. Informatics Med. Unlocked 41: 101330.

Akinlolu, O.S., Fatoki, T.H., and Momodu, D.U. (2023). Hematological and Hypoglycemic Effects of Ethanolic Extract of *Annona muricata* Ripe Fruits Pulp on Streptozotocin-induced Diabetes in Rats: *In vivo* and *In silico* Studies. J. Complement. Altern. Med. Res. 21(2): 32–42.

Apeh, V.O., Adegboyega, A.E., Chukwuma, I.F., Ugwah-Oguejiofor, C.J., Aja, P.M., Ofeimun, J.O., Ale, B.A., Johnson, G.I., Ebenyi, L.N., Iwaloye, O., Ejembi, S.A., Ezugworie, F.N., and Johnson, T.O. (2023). An *insilico* study of bioactive compounds of Annona muricata in the design of ani-prostate cancer agent: MM/GBSA, pharmacophore modeling and ADMET parameters. Informatics Med. Unlocked 43: 101377.

Arnott, J.A., and Planey, S.L. (2012). The influence of lipophilicity in drug discovery and design. Expert Opinion on Drug Discovery 7(10): 863–875.

Asangani, I.A., Rasheed, S.A., Nikolova, D.A., Leupold, J.H., Colburn, N.H., Post, S., and Allgayer, H. (2008). MicroRNA-21 (miR-21) post-transcriptionally downregulates tumor suppressor Pdcd4 and stimulates invasion, intravasation and metastasis in colorectal cancer. Oncogene 27: 2128–2136.

Bowers, K.J., Chow, E., Xu, H., Dror, R.O., Eastwood, M.P., Gregersen, B.A., Klepeis, J.L., Kolossvary, I., Moraes, M.A., Sacerdoti, F.D., Salmon, J.K., Shan, Y., and Shaw, D.E. (2006). Scalable algorithms for molecular dynamics simulations on commodity clusters. In Proceedings of the 2006 ACM/IEEE conference on Supercomputing. Association for Computing Machinery, Tampa, Florida, p. 84.

Clarke, D.J.B., Kuleshov, M.V., Schilder, B.M., Torre, D., Duffy, M.E., Keenan, A.B., Lachmann, A., Feldmann, A.S., Gundersen, G.W., Silverstein, M.C., Wang, Z., and Ma'ayan, A. (2018). eXpression2Kinases (X2K) Web: linking expression signatures to upstream cell signaling net-

works. Nucleic Acids Res. 46(W1): 171–179.
Coimbra, J.T., Feghali, R., Ribeiro, R.P., Ramos, M.J., and Fernandes, P.A. (2021). The importance of intramolecular hydrogen bonds on the translocation of the small drug piracetam through a lipid bilayer. RSC Adv. 11(2): 899–908.
Coria-Tellez, A.V., Montalvo-Gonzalez, E., Yahia, E.M., and Obledo-Vazquez, E.N. (2018). *Annona muricata*: A comprehensive review on its traditional medicinal uses, phytochemicals, pharmacological activities, mechanisms of action and toxicity. Arabian J. Chem. 11: 662–691.
Daina, A., Michielin, O., and Zoete, V. (2017). SwissADME: a free web tool to evaluate pharmacokinetics, drug-likeness and medicinal chemistry friendliness of small molecules. Sci. Rep. 7(1): 42717.
Drishya, G., Nambiar, J., Shaji, S.K., Vanuopadath, M., Achuthan, A., Kumar, A., Alias, A., Sherif, A., Joseph, C., Divya, P., Kumar, D.S., Bose, C., Nair, S.V., Sudarslal, S., Kumar, G.B., Lakshmi, S., and Nair, B.G. (2020). RECK and TIMP-2 Mediate Inhibition of MMP-2 and MMP-9 by *Annona muricata*. J. Biosci. 45: 89.
Eberhardt, J., Santos-Martins, D., Tillack, A.F., and Forli, S. (2021). AutoDock Vina 1.2.0: New Docking Methods, Expanded Force Field, and Python Bindings, J. Chem. Inf. Model 61(8): 3891–3898.
Fatoki, T.H., Balogun, C.T., Oluwadare, O.T., Famusiwa, C.D., Oyebiyi, O.R., Ejimadu, B.A., Lawal, O.E., Amosun, B.E., Adeyeye, T.O., and Falode, J.A. (2023). *In Silico* Evaluation of Nutri-Pharmacological Potentials of Phytochemicals in Sorghum (Sorghum bicolor) Grains. J. Food Bioact. 23: 58–67.
Fatoki, T.H., Faleye, B.C., Nwagwe, O.R., Awofisayo, O.A., Adeseko, C.J., Jeje, T.O., Ayenero, M.E., Fatoki, J.M., Akinlolu, O.S., Momodu, D.U., Enibukun, J.S., and Omuekwu, N.F. (2024). Friedelin Could Moderately Modulate Human Carbonic Anhydrases: An in Silico Study. Biointerface Res. Appl. Chem. 14(2): 49.
Fatoki, T.H. (2023). Human adenovirus DNA polymerase is evolutionarily and functionally associated with human telomerase reverse transcriptase based on in silico molecular characterization that implicate abacavir and zidovudine. Front. Bioinform. 3: 1123307.
Fatoki, T.H. (2022). Effect of pH on structural dynamics of HMGCoA reductase and binding affinity to β-sitosterol. J. Biomol. Struct. Dyn. 41(10): 4398–4404.
Galindo-Hernandez, O., Cordova-Guerrero, I., Diaz-Rubio, L.J., Pulido-Capiz, A., Diaz-Villanueva, J.F., Castaneda-Sanchez, C.Y., Serafin-Higuera, N., and Garcia-Gonzalez, V. (2019). Protein translation associated to PERK arm is a new target for regulation of metainflammation: A connection with hepatocyte cholesterol. J. Cell Biochem. 120: 4158–4171.
Gavamukulya, Y., Abou-Elella, F., Wamunyokoli, F., and AEl-Shemy, H. (2014). Phytochemical Screening, Anti-Oxidant Activity and in Vitro Anticancer Potential of Ethanolic and Water Leaves Extracts of *Annona muricata* (Graviola). Asian Pac. J. Trop. Med. 7: S355–S363.
González-Ortiz, A., Pulido-Capiz, A., Castañeda-Sánchez, C.Y., Ibarra-López, E., Galindo-Hernández, O., Calderón-Fernández, M.A., López-Cossio, L.Y., Díaz-Molina, R., Chimal-Vega, B., Serafín-Higuera, N., Córdova-Guerrero, I., and García-González, V. (2022). eIF4A/PDCD4 Pathway, a Factor for Doxorubicin Chemoresistance in a Triple-Negative Breast Cancer Cell Model. Cells 11: 4069.
Hadisaputri, Y.E., Habibah, U., Abdullah, F.F., Halimah, E., Mutakin, M., and Abdulah, R. (2021). Antiproliferation Activity and Apoptotic Mechanism of Soursop (*Annona muricata* L.) Leaves Extract and Fractions on MCF7 Breast Cancer Cells. Breast Cancer Targets Ther. 13: 447–457.
Hwang, S.K., Minai-Tehrani, A., Lim, H.T., Shin, J.Y., An, G.H., Lee, K.H., Park, K.R., Kim, Y.S., Beck, G.R. Jr, Yang, H.S., and Cho, M.H. (2010). Decreased level of PDCD4 (programmed cell death 4) protein activated cell proliferation in the lung of A/J mouse. J. Aerosol. Med. Pulm. Drug Deliv. 23: 285–293.
Hwang, S.K., Jeong, Y.J., and Chang, Y.C. (2020). PDCD4 inhibits lung tumorigenesis by the suppressing p62-Nrf2 signaling pathway and upregulating Keap1 expression. Am. J. Cancer Res. 10: 424–439.
Ibraheem, O., Fatoki, T.H., Enibukun, J.M., Faleye, B.C., and Momodu, D.M. (2019). *In Silico* Toxicological Analyses of Selected Dumpsite Contaminants on Human Health. Nova Biotechnol. Chim. 18(2): 144–153.
Indrawati, L., Ascobat, P., Bela, B., Abdullah, M., and Surono, I.S. (2017). The Effect of an *Annona muricata* Leaf Extract on Nutritional Status and Cytotoxicity in Colorectal Cancer: A Randomized Controlled Trial. Asian Pac. J. Clin. Nutr. 26: 606–612.
Jin, H., Kim, T.H., Hwang, S.K., Chang, S.H., Kim, H.W., Anderson, H.K., Lee, H.W., Lee, K.H., Colburn, N.H., Yang, H.S., Cho, M.H., and Cho, C.S. (2006). Aerosol delivery of urocanic acid-modified chitosan/programmed cell death 4 complex regulated apoptosis, cell cycle, and angiogenesis in lungs of K-ras null mice. Mol. Cancer Ther. 5: 1041–1049.
Keiser, M.J., Roth, B.L., Armbruster, B.N., Ernsberger, P., Irwin, J.J., and Shoichet, B.K. (2007). Relating protein pharmacology by ligand chemistry. Nat. Biotech. 25(2): 197–206.
Kim, J.Y., Dao, T.T.P., Song, K., Park, S.B., Jang, H., Park, M.K., Gan, S.U., and Kim, Y.S. (2018). *Annona muricata* Leaf Extract Triggered Intrinsic Apoptotic Pathway to Attenuate Cancerous Features of Triple Negative Breast Cancer MDA-MB-231 Cells. Evid.-Based Complement. Altern. Med. 2018: 916.
Kostal, J. (2016). Computational chemistry in predictive toxicology: Status quo et quo vadis? In: Fishbein, J.C., and Heilman, J.M. (Ed.). Advances in Molecular Toxicology, Vol. 10. Elsevier, pp. 139–186.
Mao, X.H., Chen, M., Wang, Y., Cui, P.G., Liu, S.B., and Xu, Z.Y. (2017). MicroRNA-21 regulates the ERK/NF-kappaB signaling pathway to affect the proliferation, migration and apoptosis of human melanoma A375 cells by targeting SPRY1, PDCD4 and PTEN. Mol. Carcinog. 56: 886–894.
Martin, P., Giardiello, M., McDonald, T.O., Rannard SP, , and Owen, A. (2013). Mediation of in vitro cytochrome P450 activity by common pharmaceutical excipients. Mol. Pharm. 10: 2739–2748.
McCammon, J.A., and Karplus, M. (2002). Molecular dynamics simulations of biomolecules. Nat. Struct. Biol. 9(9): 646–652.
Moghadamtousi, S.Z., Kadir, H.A., Paydar, M., Rouhollahi, E., and Karimian, H. (2014). *Annona muricata* Leaves Induced Apoptosis in A549 Cells through Mitochondrial-Mediated Pathway and Involvement of NF-κB. BMC Complement. Altern. Med. 14: 1–13.
Morris, G.M., Huey, R., Lindstrom, W., Sanner, M.F., Belew, R.K., Goodsell, D.S., and Olson, A.J. (2009). AutoDock4 and AutoDockTools4: automated docking with selective receptor flexibility. J. Comput. Chem. 30(16): 2785–2791.
Mutakin, M., Fauziati, R., Fadhilah, F.N., Zuhrotun, A., Amalia, R., and Hadisaputri, Y.E. (2022). Pharmacological Activities of Soursop (*Annona muricata* Lin.). Molecules 27: 1201.
Nwonuma, C.O., Balogun, E.A., and Gyebi, G.A. (2023). Evaluation of Antimalarial Activity of Ethanolic Extract of *Annona muricata* L.: An *in vivo* and an *in silico* Approach. J. Evid.-Based Integr. Med. 28: 1–30.
Parks, W.C., Wilson, C.L., and Lopez-Boado, Y.S. (2004). Matrix metalloproteinases as modulators of inflammation and innate immunity. Nat. Rev. Immunol. 4: 617–629.
Pieme, A.A., Kumar, G.G., Dongmo, S.S., Moukette, M.M., Boyoum, F.F., Ngogang, Y.Y., and Saxena, K.K. (2014). Antiproliferative Activity and Induction of Apoptosis by *Annona muricata* (Annonaceae) Extract on Human Cancer Cells. BMC Complement. Altern. Med. 14: 1–10.
Pin, G., Huanting, L., Chengzhan, Z., Xinjuan, K., Yugong, F., Wei, L., Shifang, L., Zhaojian, L., Kun, H., Weicheng, Y., Yingying, L., Yongming, Q., and Yanan, Y. (2020). Down-Regulation of PDCD4 Promotes Proliferation, Angiogenesis and Tumorigenesis in Glioma Cells. Front. Cell Dev. Biol. 8: 593685.
Rentzsch, R., and Renard, B.Y. (2015). Docking small peptides remains a great challenge: an assessment using AutoDock Vina. Brief Bioinform. 16(6): 1045–1046.
Schrödinger. (2018). Schrödinger release 2018-3. Desmond molecular dynamics system, D.E. Shaw research, New York, NY, 2018. Maestro Desmond Interoperability Tools, Schrödinger, New York, NY, 2018.
Schrödinger. (2019). What do all the Prime MM-GBSA energy properties mean? www.schrodinger.com/kb/1875.
Shibahara, K., Asano, M., Ishida, Y., Aoki, T., Koike, T., and Honjo, T. (1995). Isolation of a novel mouse gene MA-3 that is induced upon programmed cell death. Gene. 166: 297–301.
Shivakumar, D., Williams, J., Wu, Y., Damm, W., Shelley, J., and Sherman, W. (2010). Prediction of Absolute Solvation Free Energies using Molecular Dynamics Free Energy Perturbation and the OPLS Force Field. J. Chem. Theory Comput. 6: 1509–1519.
Singh, M., Garg, N., Venugopal, C., Hallett, R., Tokar, T., McFarlane, N.,

Mahendram, S., Bakhshinyan, D., Manoranjan, B., Vora, P., Qazi, M., Arpin, C.C., Page, B., Haftchenary, S., Rosa, D.A., Lai, P.S., Gomez-Biagi, R.F., Ali, A.M., Lewis, A., Geletu, M., Murty, N.K., Hassell, J.A., Jurisica, I., Gunning, P.T., and Singh, S.K. (2015). STAT3 pathway regulates lung-derived brain metastasis initiating cell capacity through miR-21 activation. Oncotarget 6(29): 27461–27477.

Suhandi, C., Bagaskhara, P.P., Puspita, R.I.S., Amalia, S.H., Azzahra, A.B., and Citraloka, Z.G. (2022). In Silico Study of Compound Extract in Soursop Plant (Annona muricata) as ACE Inhibitor in Hypertension Disease. Indones. J. Comput. Biol 1(1): 7–15.

Szklarczyk, D., Gable, A.L., Nastou, K.C., Lyon, D., Kirsch, R., Pyysalo, S., Doncheva, N.T., Legeay, M., Fang, T., Bork, P., Jensen, L.J., and von Mering, C. (2021). The STRING database in 2021: Customizable protein#x2013;protein networks, and functional characterization of user-uploaded gene/measurement sets. Nucleic Acids Res. 49: D605–D612.

Tao, A., Huang, Y., Shinohara, Y., Caylor, M.L., Pashikanti, S., and Xu, D. (2019). ezCADD: A Rapid 2D/3D Visualization-Enabled Web Modeling Environment for Democratizing Computer-Aided Drug Design. J. Chem. Inf. Model 59: 18–24.

Trott, O., and Olson, A.J. (2010). AutoDock Vina: improving the speed and accuracy of docking with a new scoring function, efficient optimization, and multithreading. J. Comput. Chem. 31(2): 455–61.

Wang, D., Hou, Q., Zhao, L., Gao, J., Xiao, Y., and Wang, A. (2019). Programmed cell death factor 4 enhances the chemosensitivity of colorectal cancer cells to Taxol. Oncol. Lett. 18: 1402–1408.

Wong, F., Krishnan, A., Zheng, E.J., Stark, H., Manson, A.L., Earl, A.M., Jaakkola, T., and Collins, J.J. (2022). Benchmarking Al-phaFold-enabled molecular docking predictions for antibiotic discovery. Mol. Syst. Biol. 18: e11081.

Yang, C., Gundala, S.R., Mukkavilli, R., Vangala, S., Reid, M.D., and Aneja, R. (2015). Synergistic Interactions among Flavonoids and Acetogenins in Graviola (*Annona muricata*) Leaves Confer Protection against Prostate Cancer. Carcinogenesis 36: 656–665.

Zhang, D., Shi, Z., Li, M., and Mi, J. (2014). Hypoxia-induced miR-424 decreases tumor sensitivity to chemotherapy by inhibiting apoptosis. Cell Death Dis. 5: e1301.

Zhang, X., Perez-Sanchez, H., and Lightstone, F.C. (2017). A Comprehensive Docking and MM/GBSA Rescoring Study of Ligand Recognition upon Binding Antithrombin. Curr. Topics Med. Chem. 17: 1631–1639.

Zhen, Y., Li, D., Li, W., Yao, W., Wu, A., Huang, J., Gu, H., Huang, Y., Wang, Y., Wu, J., Chen, M., Wu, D., Lyu, Q., Fang, W., and Wu, B. (2016). Reduced PDCD4 expression promotes cell growth through PI3K/Akt signaling in non-small cell lung cancer. Oncol. Res. 23: 61–68.